Journal of Engineering Science and Technology
Vol. 13, No. 3 (2018) 755 - 777

MECHANICAL AND TRIBOLOGICAL BEHAVIOUR OF STIR CAST ALUMINIUM/BORON CARBIDE/FLY ASH COMPOSITES

X. CANUTE*, M. C. MAJUMDER

Department of Mechanical Engineering, National Institute of Technology, Durgapur, India
*Corresponding Author:xcanute@gmail.com

Abstract

A new attempt has been made in the current research work to produce hybrid composites with aluminium A356 alloy as matrix and boron carbide powder (4%), fly ash (4%) as reinforcements by the stir casting method. High-temperature tribological behavior of aluminium boron carbide fly ash composites using the pin on disc method with pin heating setup studied in this investigation. Fly ash particles added as a secondary reinforcement material due to its notable mechanical, metallurgical and tribological properties. Mechanical tests like tensile test, micro hardness test and microstructure studies were conducted. The significance of load, sliding velocity and temperature on the wear rate of the hybrid composites was evaluated. The test results showed considerable development in the mechanical properties and uniform particle distribution in the matrix. The tensile and compression strength of the hybrid composites increased considerably whereas ductility reduced. The morphology of pin surface studied through a high-resolution scanning electron microscope. Analysis of variance method used to explore the effect of wear parameters on the wear rate. The results of the investigation revealed that the load had the highest significance, followed by temperature and sliding velocity. The wear rate increase with the rise in applied load and temperature and decrease with increase in sliding velocity. The developed composites can be used in the production of automobile parts which require high wear and thermal resistance.

Keywords: HMMC, Wear, Friction, ANOVA, SEM, Delamination.

1. Introduction

Eco-friendly composite materials possess superior thermal and biodegradable properties. Aluminium composite materials are widely preferred in automotive and aeronautical industries due to its excellent mechanical, metallurgical and tri-

Nomenclatures

S/N	Signal to noise ratio, dB

Greek Symbols

α	Peak, spectral line
λ	Ångstroms, 1 Å = 0.1 nm, λ=1.5406 Å
μ	Microns
ρ	Density, gms/cc

Abbreviations

ALFA	Aluminium Fly Ash
ANOVA	Analysis of Variance
ASTM	American Society of Testing Materials
BHN	Brinell Hardness Number
DOE	Design of Experiments
EDS	Energy Dispersive x-ray Spectroscopy
HMMC	Hybrid Metal Matrix Composites
MMC	Metal Matrix Composites
POD	Pin On Disc
SEM	Scanning Electron Microscope
UTS	Ultimate Tensile Strength
VHN	Vickers Hardness Number
XRD	X-Ray Diffraction

bological characteristics. The technology and cost of metal matrix composites (MMC) depend on processing methods and its effectiveness [1]. The properties of hybrid metal matrix composites (HMMC) were superior to aluminium cast alloys and particle reinforced metal matrix composites [2, 3]. Aluminium matrix composites have excellent toughness and strength [4]. Aluminium boron carbide composites used in the production of neutron absorbers and armour plate materials. These composites have good strength and wear resistance [5].

Boron carbide is a worthy choice for the reinforcement because of its high hardness. Fly ash has less density and better mechanical properties. Fly ash is eco-friendly reinforcement material. Precipitator fly ash has a high density (2.0-2.5 gms/cc) compared to cenosphere fly ash (1.0 gms/cc). Large castings are produced by stir casting method. Stir casting route selected for processing aluminium composites due to its low processing cost. Melt stiring method promote wettability, homogeneous particle distribution in the matrix and aid in forming fine equiaxed grain structure. The combined methodology involving compocasting and squeeze casting yield a better casting with less porosity [6]. Aluminium fly ash composites (ALFA) have distinct advantages like property improvement, environmental benefits, cost reduction and material savings. Energy consumption, cost and emission were greatly reduced by aluminium fly ash composites. The important applications of aluminium fly ash composites are brake rotors and pistons. ALFA composites with low fly ash percentage are used in the production of various automotive parts like manifolds, brackets, housings, household extruded parts and yard tool covers [7]. The addition of fly ash as reinforcement material increase yield

strength, compression strength and hardness. The ductility of the fly ash composites reduces with the escalation in the reinforcement content of particles and decreases with an increase in the fly ash particle size [8]. The occurrence of firm ceramic phase susceptible to localized crack initiation and augmented embrittlement at interface between matrix and reinforcement particles [9]. The decrease in ductility attributed to the formation of the cavities that nucleate during the plastic straining of the reinforcement particles [10, 11].

The chemical composition and microstructure of aluminium fly ash composites produced depend on the chemical reaction between the aluminium matrix and reinforcement particles [12]. The main reaction products formed during the synthesis of the aluminium fly ash HMMC are aluminium oxide, silicon, iron and magnesium oxide [13, 14].

The tribological properties of aluminium fly ash composites were higher compared with aluminium cast alloy [15]. Few researchers incorporated fly ash content in aluminium matrix up to 17% [16]. The hardness, strength composites increases with fly ash content [17]. The tensile and compression properties also increase by adding fly ash particles and aluminium oxide [18, 19].

Lashgari et al. [20] examined the influence of strontium on improving wear resistance in aluminium boron carbide stir cast composites with 10% reinforcement. They proved that adding strontium to aluminium boron carbide composites increase wear resistance. The addition of boron carbide in Al-Si-Mg alloy matrix yield improved mechanical properties. The boron carbide particles were uniformly dispersed in the aluminium matrix [21]. Kalaiselvan et al. [22] examined the effect of boron carbide particles (20 μm) with varying weight fractions (2%, 4%, 6% and 8%) in A359 alloy through stir casting method. The experimental results revealed that the A359/B_4C/8p composites have high hardness and tensile strength.

Inhomogeneous distribution of particle and porosity are the major difficulties in producing cast ALFA composites. The main cause of inhomogeneous distribution is due to the poor wettability of boron carbide particles with the aluminium matrix. These problems were reduced by controlling process parameters and proper design of the stirrer [23]. Potassium flurotitanate (K_2TiF_6) added as a flux to promote wettability. It forms a reaction layer of titanium carbide and titanium diboride at the interface [24]. Coated boron carbide and fly ash particles improve wettability**.** The particle size and fly ash composition significantly influence the wear parameters. The effect of tribological parameters of Al-Si/12p/FA/15p composites was investigated previously. Wear rate increase with the rise in load and sliding velocity. The tribological properties were reduced considerably by the increased content of fly ash particles [25].

Wear rate and hardness of Al-SiC-fly ash composites increase with an increased silicon carbide content [26]. Uthayakumar et al [27] produced AA6351/FA composites and investigated the effect of the control factors such as load, sliding velocity and reinforcement content by grey relational analysis technique and ANOVA method. The load had the utmost influence on the wear rate when compared with sliding velocity and reinforcement content. The tribological behaviour of ALFA composites with narrow range particle size was comparatively higher than wide range size [28].

The methods available for high temperature pin on disc wear tests are chamber heating and pin heating method. Pin heating method is preferred because high temperatures reached within a short time period.

The effect of load, sliding speed and temperature on the wear of stainless steel studied earlier and it was concluded that frictional coefficient and surface finish increase with temperature [29]. Radhika et al. [30] studied the effect of load, sliding speed and sliding distance of Al-Al_2O_3/9p/Gr/3p composites and concluded that sliding distance significant effect when compared to other parameters.

The influence of temperature, load and sliding velocity on the tribological properties of AA7075/SiC/10p composites with reinforcement particle size of 120 microns and temperature range of 30°,60° and 90°C was investigated. It was concluded that load and temperature have a significant effect on the wear rate than sliding velocity [31]. The high temperature tribological behaviour of Al6063/TiB_2 composites under different load and temperature was studied earlier. The wear rate of composites at high temperature was higher when compared to test conducted at room temperature. The wear resistance also increases with a rise in the titanium diboride content [32].

Based on the above literature review, a research gap has been identified in the production of high temperature wear resistant composite materials. The high temperature tribological behaviour of aluminium boron carbide fly ash composites has been carried out in this research work.

2. Materials and Methods

2.1. Material selection

Aluminium A356 possesses good castability, corrosion resistance and machinability and weldability characteristics. Aluminium composites have extensive applications like armour plates, track shoes, cylinder liners, cylinder block and drive shafts [33]. The important advantages of aluminium A356 casting alloy are greater elongation, higher strength, good thermal stability and corrosion resistance. The composition of aluminium alloy A356 alloy is shown in Table 1. The composition of fly ash is shown in Table 2.

Table 1. Composition of aluminium alloy A356 alloy.

Element	Cu	Mg	Mn	Si	Fe	Zn	Ti	Al
Weight %	0.20	0.25-0.45	0.10	6.5-7.5	0.20	0.10	0.20	Bal

Table 2. Composition of fly ash.

Element	Al_2O_3	SiO_2	Fe_2O_3	CaO	TiO_2	Other elements
Weight,%	25.52	51.60	8.94	6.15	0.51	Balance

The aluminium A356 alloy was mixed with boron carbide powder (4%) by the stir casting method. Boron carbide powder (63 microns) and fixed weight percentage (4%) of fly ash particles (10-100 microns) were used as the reinforcement material. Magnesium powder was added to increase strength and

reduce casting fluidity and surface tension in aluminium. Strontium based master alloy Al10Sr (0.03%) was used to improve mechanical properties and aid in grain modification. The composition of fly ash includes silica, alumina, calcium and magnesium oxide.

2.2. Material characterisation

The analysis of X-Ray diffraction studies shows elements like SiO_2, Fe_2O_3, Al_2O_3, CaO, TiO2 and SO_3. The SEM and EDS of A356 cast alloy are shown in Figs.1 and 2. SEM, EDS and XRD images of fly ash particles are shown in Figs. 3, 4 and 5. The particle shape of fly ash is mostly spherical as revealed by the SEM image. The elements revealed in EDS analysis of fly ash particles are magnesium, oxygen, titanium, calcium, aluminium, silicon and iron. The SEM image of Al A356 cast alloy indicates the presence of grooves and aluminium-silicon-strontium compounds with Al and Si solutes.

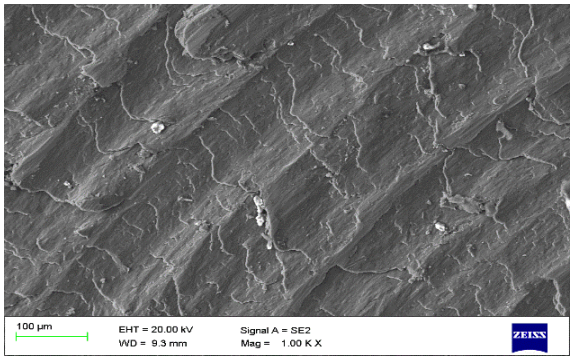

Fig. 1. SEM image of Al cast alloy.

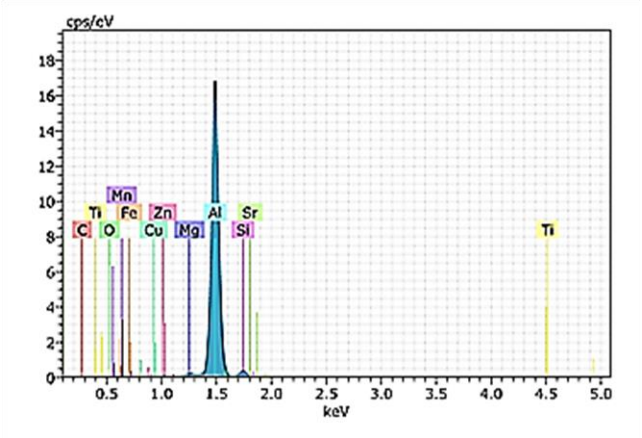

Fig. 2. EDS image of Al cast alloy.

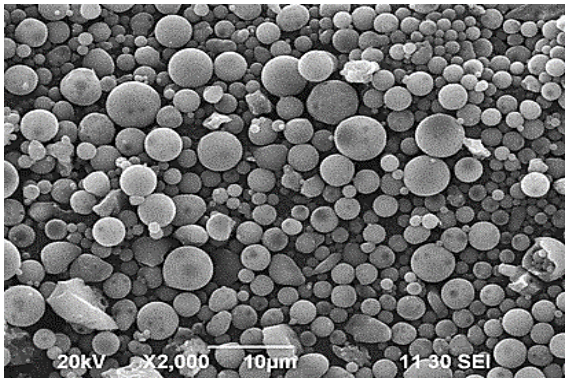

Fig. 3. SEM image of fly ash.

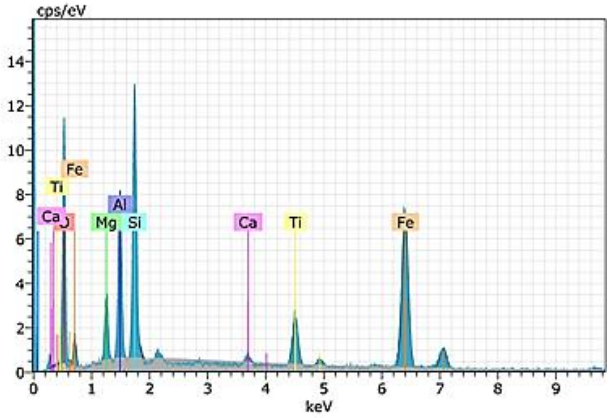

Fig. 4. EDS image of fly ash.

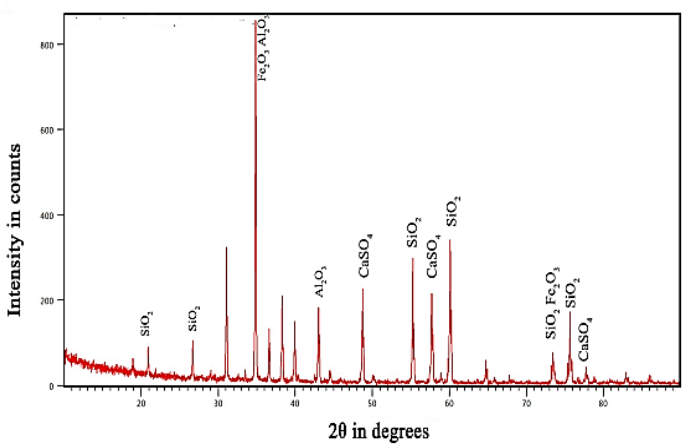

Fig. 5. XRD image of fly ash.

2.3. Production of hybrid composites

The stir casting route was chosen to process Al-B_4C-Fly ash composites due to its low cost and suitability of producing large castings. Calculated amount of billet was charged into the stir-casting furnace and the temperature was increased to 850°C. Boron carbide powder and fly ash powder is heated to 400° C for three hours and added to the melt. The temperature decreased gradually till it reaches a semisolid state. Hexachloroethane tablets were added to melt to remove the entrapped air and porosity. Then the reinforcement particles were added to the liquid melt. Potassium flurotitatnate powder, Al-Sr master alloy and magnesium were added in required proportions. The slurry is heated to full liquid state and temperature upheld at 750°C. The melt was agitated continuously for 15 minutes. The pouring temperature was kept at 720°C.

2.4. Wear test details

Wear tests of Al-B_4C-FA composites were performed by POD machine as per ASTM G99 standards. POD Wear and Friction Monitor are publicized in Figs. 6 and 7 illustrate the pin heating arrangement. The specimen was lapped by 1200 grit paper. The weight of the composite pin before and after test was noted by a digital electronic balance (Model: SHIMADZU AUY 220) with an accuracy of 0.1mg. The pin is inserted in the collet which is surrounded by heater coil. The sliding distance was kept constant for corresponding sliding velocities 1 m/s, 2 m/s, 3 m/s respectively. The wear test details are given in Table 3.

Table 3. Wear test details.

Parameter	Description
Material of Pin	Al/B_4C/4p/FA/4p
Dimension of Pin	Φ10mm×27 mm
Disc Material	EN32 Case hardening steel
Dimensions of disc	Φ165 mm×8 mm thick
Hardness of disc	62 HRC
Sliding velocity (m/s)	1 m/s, 2 m/s,3 m/s
Sliding Time	15 minutes
Load (N)	10,20,30
Sliding Distance(m)	900,1800,2700
Track Diameter	110 mm

The wear rate (WR) was computed as shown in Eq. (1).

$$WR = \frac{\Delta W}{\rho \times D} \text{ mm}^3/\text{m} \quad (1)$$

where ρ = Density of the composite (gms/cm^3), ΔW=Weight loss (gms) and D = Sliding distance (m)

Fig. 6. POD wear and friction monitor.

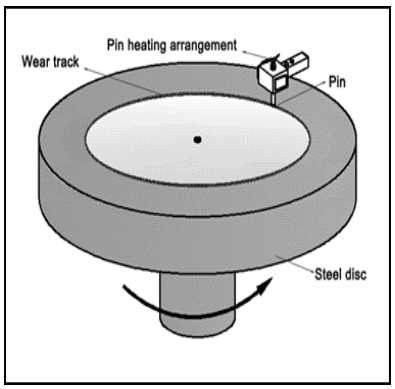

Fig. 7. POD pin heating setup.

2.5. Tensile test

The tensile tests were done by a universal material tester per ASTM E8 standards at a crosshead speed of 1 mm/min.

2.6. Compression test

The specimen is machined to 13 mm diameter and length 26 mm with aspect ratio 1:2 as per ASTM E9 standards. The specimen was placed between two flat dies, which was lubricated with graphite powder to reduce friction between the surfaces of the die and test specimen.

2.7. Hardness test

The test was carried out with a micro-hardness tester (Model: Mitutoyo MVKH1). The test was carried out with test load of 50g, 20 seconds dwell time and indentation time of 15 seconds. The results of hardness values were plotted.

2.8. Optical microscopy

The sample preparation consisted of polishing with emery paper from 600 to 1200 grit size, aluminium oxide suspension and diamond paste. Then the specimen examined through the optical microscope (Zeiss Axiovert 25VA inverted Metallurgical microscope) at different magnifications (I00X, 200X and 500X).

2.9. Scanning Electron Microscopy

SEM micrographs were taken by the scanning electron microscope (Model: JOEL USM-6390 with energy dispersive (EDX) detector.

2.10. X Ray Diffraction analysis

The XRD diffraction pattern was recorded by an X-ray diffractometer (Model: Bruker D8, Germany). The machine was operated at 40 KV voltage and

30 mA using Cu Kα radiation (λ = 1.5406 Å) in the angle range of 20-80 [34]. The phases and reaction products of Al-B_4C-4FA composites were identified through XRD analysis. The XRD test specimen machined to 10 mm square with thickness of 5 mm. The specimen was ground and polished before the XRD test.

3. Experimental Plan

The parameters considered for current investigation were load, sliding velocity and temperature for this work. The process parameters and levels are shown in Table 4. The L9 orthogonal array used for this study. Load, sliding velocity and temperature is selected as control factors. Wear rate was examined as the response variable. The data analysis was carried through MINTAB 16 software. The choice of an array was based on the condition that the degrees of freedom should greater than or equal to the sum of the variables [35]. The experimental values were analyzed by ANOVA method. The experimental data were converted to signal to noise ratio. The S/N ratio is given by Eq. (2).

$$S/N = -10\, log[(1/n\ (\sum y^2)] \quad (2)$$

y is the observed data and *n* is the number of observations. The transformation of signal to noise is used for optimization of wear rate.

Table 4. Parameters and levels.

Level	Load (N), A	Sliding velocity(m/s), B	Temperature (ºC), C
1	10	1	60
2	20	2	120
3	30	3	180

4. Results and Discussion

4.1. Microstructural analysis

The microstructure of Al/4B_4C/4FA composites observed at 200X and 500X are publicized in Figs. 8 and 9. SEM image is shown in Fig. 10. The EDS image of Al/4B_4C/4FA composite is shown in Fig. 11.

The microstructure reveals that boron carbide and fly ash particles were distributed uniformly in the matrix. The microstructure shows α-aluminium particles as a fine equiaxed dendritic structure by the inclusion of strontium.

The reinforcement particles bonded to the matrix alloy. This phenomenon enhances the mechanical properties of the composites [36]. The dendritic growth of silicon is restricted at the grain boundaries. Clustering of fly ash particles is not observed [37].

High magnification SEM images reveal round shaped fly ash particles with large specific area. SEM images reveal good bonding among the aluminium, fly ash and boron carbide particles.

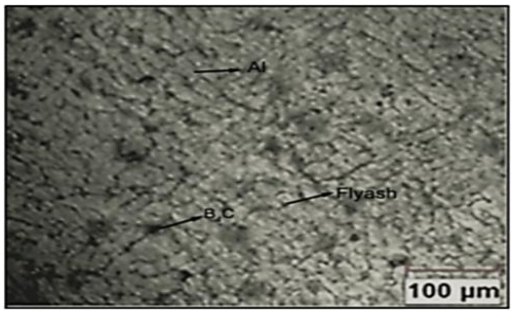

Fig. 8. Microstructure of Al/4B_4C/4FA (200X).

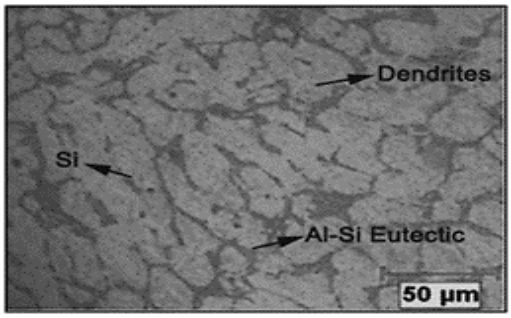

Fig. 9. Microstructure of Al/4B_4C/4FA composite (500X).

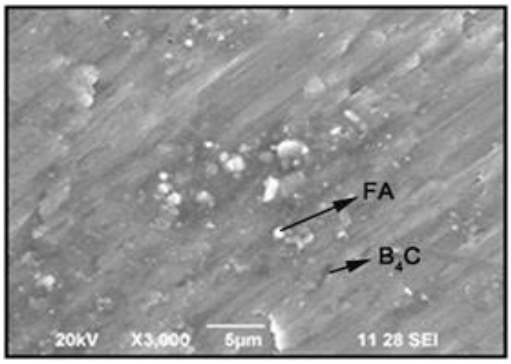

Fig. 10. SEM-Al/4B_4C/4FA (3000X).

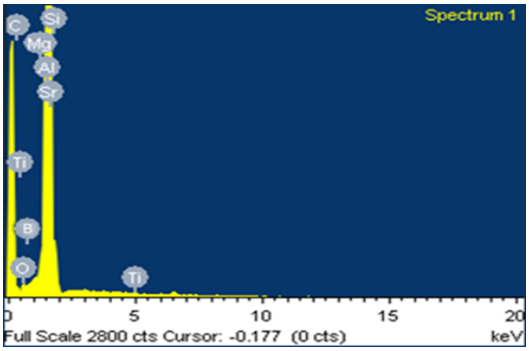

Fig. 11. EDS image of Al/4B_4C/4FA composite.

4.2. XRD studies

The results of XRD show the intensity peaks of Al, B_4C, Al_3Ti, B_2O_3, Al_4C_3, TiB_2, TiC, Fe, Si, Al_2O_3 and Al_3BC (Fig. 12). Reaction products like AlB_2 and Al_3BC, Al_4C3 were detected in the image. Due to the addition of titanium based flux, the reaction layer at the interface layer consisting of TiB_2 is formed around boron carbide particles. Al_3BC and AlB_2 was formed at 868◦C. AlB_2 is completely replaced by TiB_2 due to interfacial reactions [38]. Al_3BC is the major reaction product formed. The presence of AlB_2 phase is relatively less [39].

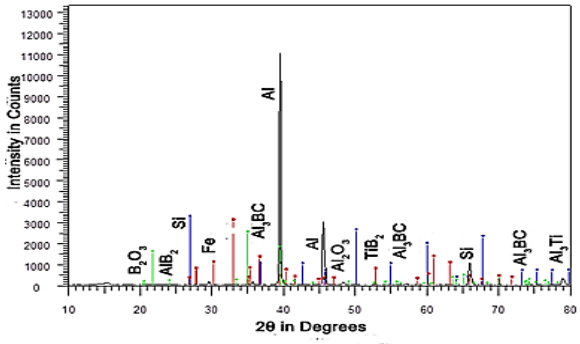

Fig. 12. XRD image of Al/4B_4C/4FA composite.

4.3. Tensile properties

Tensile properties of cast aluminium A356 and hybrid composites were evaluated. The aluminium A356 cast alloy has an ultimate tensile strength about 189 MPa with 12.22 % elongation. The value of ultimate tensile strength of hybrid composites is 16.9% higher than A356 cast alloy (Fig. 13).The increase in mechanical properties is due to alloy strengthening and reduction of grain size of the composite matrices [40]. Fly ash particles act as obstacles to dislocation movement and refinement of grain structure [41, 42].

The elongation of A356 cast alloy (12.22%) is higher than the hybrid composites (4.46%). The ductility of the hybrid composites was reduced with the addition of boron carbide particles and its strain hardening behavior. Embrittlement effect occurs due to the occurrence of the fly ash particles and it causes increased local stress concentration sites at matrix/particle interface. The reduction in ductility is also attributed by the formation of fly ash particle pore clusters [43, 44].

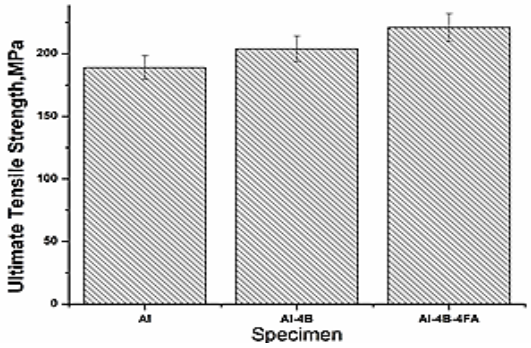

Fig. 13. Tensile test results.

4.4. Hardness

The hardness of composites improves with the addition of fly ash and strontium. The hardness plot is shown in Fig. 14. The values of Al/4B_4C-4FA composites are 31.64% more compared to A356 cast aluminium alloy and 22.11% higher compared to Al-B_4C composites. The increase in hardness is due to enhancement of strain energy caused by resistance to the plastic deformation of the boron carbide particles [45]. Fly ash particles add hardness to the aluminium composites due to alumina and silica content. Fly ash particle foster hardness and decrease density. The increase in hardness is due to dispersion strengthening of reinforcement particles, which restrict the dislocation movement [46].

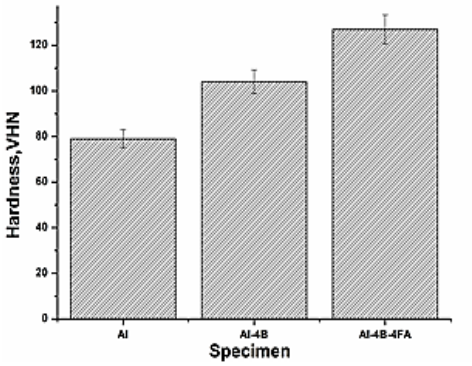

Fig. 14. Hardness of Al/4B_4C/4FA composites.

4.5. Compression strength

The compression strength of Al-B_4C-FA composites is enhanced compared to cast A356 alloy (Fig. 15). The values of Al/4B_4C/4FA composites are 10% more compared to A356 cast aluminium alloy and 4.68% higher compared to Al-B_4C composites. Good binding properties of fly ash particles promote rise improvement in compression strength and the pressure applied leads to the reduction of pores [47]. The dislocation movement in the matrix is prevented by the boron carbide particles [48]. The compressive strength is greater than the tensile strength owing to the hardening of the aluminium alloy by fly ash particles. The porosity will not have an effect on compressive strength due to the compressive force applied.

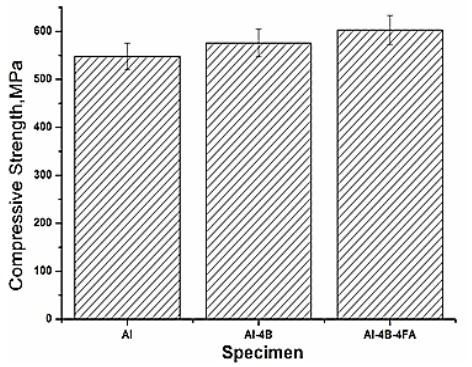

Fig. 15. Compression test of Al/4B4C/4FA composites.

4.6. Wear test results

The wear test results are shown in Table 5. The upshot of load, sliding velocity and temperature on wear rate was analyzed by MINITAB 16 software.

Table 5. Experimental results.

Trial No.	Load, N	Sliding velocity	Temperature	Wear rate	S/N Ratio
1	10	1	60	0.001556	56.1598
2	10	2	120	0.001884	54.4984
3	10	3	180	0.002473	52.1355
4	20	1	120	0.003272	49.7037
5	20	2	180	0.002942	50.6271
6	20	3	60	0.001723	55.2743
7	30	1	180	0.004530	46.8780
8	30	2	60	0.002587	51.7441
9	30	3	120	0.003259	49.7383

4.7. Effect of process parameters on response

The parameter with the highest S/N ratio gives minimum wear rate [49]. Response table for the signal to noise ratio is shown in Table 6 and means is shown in Table. 7. The main effects plot for S/N ratio is shown in Fig. 16. The main effect of plots for means is shown in Fig. 17. The load has a significant impact on wear compared to sliding velocity and temperature. The wear rate increases with applied load [50]. When sliding velocity is increased the contact time between the disc and the pin decreases. Hence the wear rate is decreased.

Table 6. Response table for signal to noise ratio.

Level	Load (A)	Sliding velocity (B)	Temperature (C)
1	54.26	50.91	54.39
2	51.87	52.29	51.31
3	49.45	52.38	49.88
Delta	4.81	1.47	4.51
Rank	1	3	2

Table 7. Response table for means.

Level	Load (A)	Sliding velocity (B)	Temperature (C)
1	0.001971	0.003119	0.001955
2	0.002646	0.002471	0.002805
3	0.003459	0.002485	0.003315
Delta	0.001488	0.000648	0.001360
Rank	1	3	2

The optimal wear rate occurs when the load is at level 1(10N), sliding velocity at level 3 (3 m/s) and temperature at level 1 (60ºC). Wear rate progresses with the applied load. Wear rate increase with the rise in temperature due to softening of

the material. Wear rate decreases when the sliding velocity is increased from 2 m/s to 3 m/s. Abrasive wear increases with an increase in temperature. Hardness, flow stress and yield strength decrease when temperature increases [51].

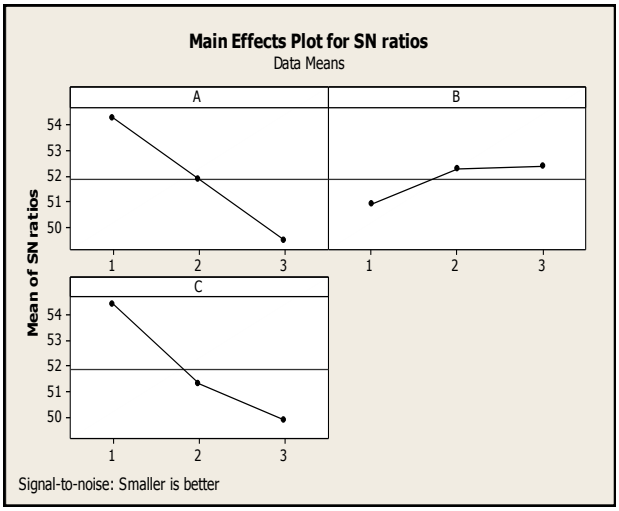

Fig. 16. Main effects plot for S/N ratio.

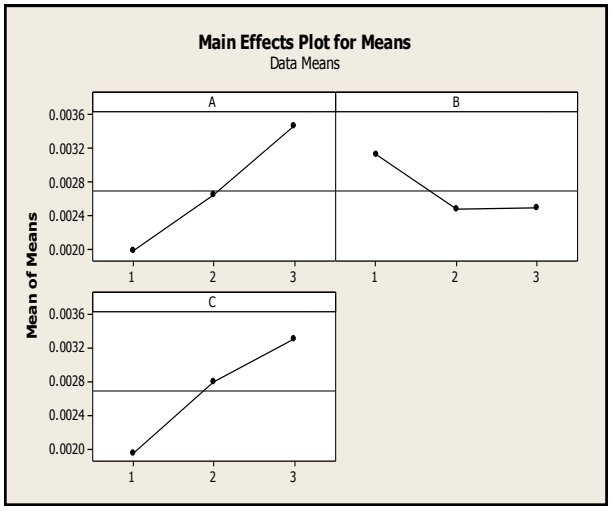

Fig. 17. Main effects plot for means.

4.8. Analysis of variance and influence of parameters

ANOVA was performed with a 95 % confidence level and 5% significance level. The influence of individual parameters is shown in Table. 8. The applied load has the greater statistical influence (47.14%) and followed by temperature (40 %) and sliding velocity (11.42%). The values of regression coefficient (R^2) and adjusted regression coefficient (R^2adj.) for wear rate are 99.19% and 96.76% respectively.

Table 8. Analysis of variance for wear rate (WR).

Source	DF	Seq. SS	F	P	Pr (%)
Load,(A)	2	0.0000033	58.40	0.017	47.14
Sliding velocity, (B)	2	0.0000008	14.44	0.065	11.42
Temperature,(C)	2	0.0000028	49.66	0.020	40.00
Error	2	0.0000001			1.42
Total	8	0.0000070			

4.9. Multiple regression analysis

A regression equation was generated by the correlation of process parameters like load, sliding velocity and temperature. Regression equation is given by Eq. (3), which establishes the equation between the parameters like load, sliding velocity and temperature

$$WR = 0.0004788 + 0.0007438A - 0.0003171B + 0.0006798C \quad (3)$$

The regression equation predicts the wear rate for aluminium boron carbide fly ash composites. From the above relation, it was observed that the coefficient associated with load and temperature was positive.

This clearly reveals that as load and temperature increases, the wear rate of the hybrid composite also increases. The negative coefficient of sliding velocity reveals that an increase in sliding velocity decreases the wear rate.

4.10. Analysis of worn pin surface

SEM analysis of the worn pin surfaces is shown in Figs. 18, 19 and 20. Fine and shallow grooves formed at low applied load and speed due to abrasive wear. The particles of the steel disc penetrate into the pin and hence wear on the pin is accelerated.

Hard reinforcement particles remove material from the wear surface when the load increases, which is attributed to the delamination. Due to softening of the material, extra material is removed from the pin at high temperature. The delamination wear is more at the higher temperature. This phenomenon proved and validated by the earlier researcher [52].

The hardness of the aluminium matrix decreases due to the recrystallization and then the aluminium will be removed by the counterpart disc. The reinforcements distributed uniformly in the aluminium matrix have high bonding strengths with the matrix and can successfully endure the external applied load, which enhances the wear resistance of the composites [53].

The phenomenon of adhesive wear is predominant at maximum load, 30 N. Wear tracks tend to disappear at this juncture. Fly ash and boron carbide particles gather at the boundaries of α-aluminium dendrites in the casting [54]. SEM image of the worn out pin surface at L = 20 N, S = 3 m/s, T=60ºC is shown in Fig. 21.

The grooves widen with increased load. EDS image (Fig. 22) reveals carbon, iron, silicon, boron, silicon, magnesium and aluminium. Mixed mechanical layer exhibits extreme hardness. The amount of wear debris formed is higher at increased load. Also the width of the grooves is also larger [55]. The mechanism of wear rate is greatly affected by the two sliding surface interaction. The heat due

to friction between the surface of the pin and disc increases with the load and duration of the test [56].

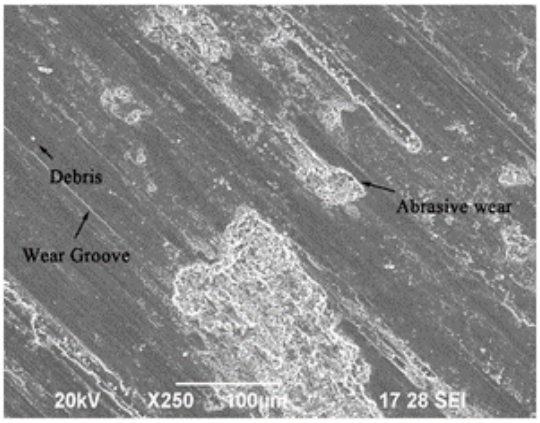

Fig. 18. SEM image (10 N, 2 m/s, 120ºC).

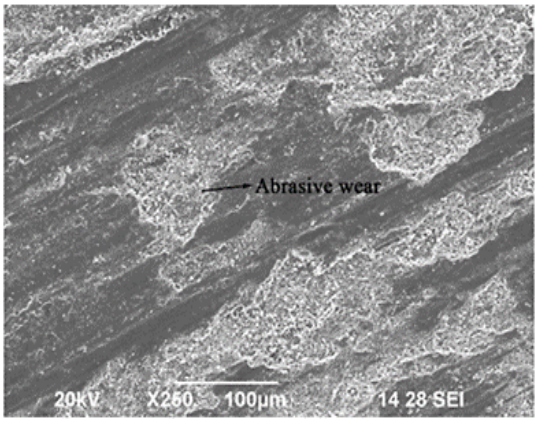

Fig. 19. SEM image (20 N, 2 m/s, 180ºC).

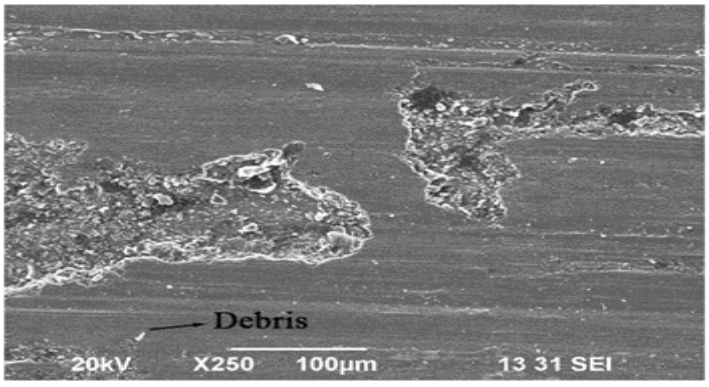

Fig. 20. SEM image (30 N, S = 2 m/s and T = 60 ºC).

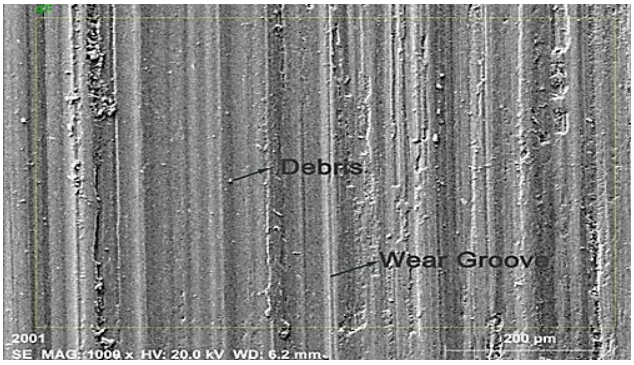

Fig. 21. SEM image (L = 20 N, S = 3 m/s and T=60º C).

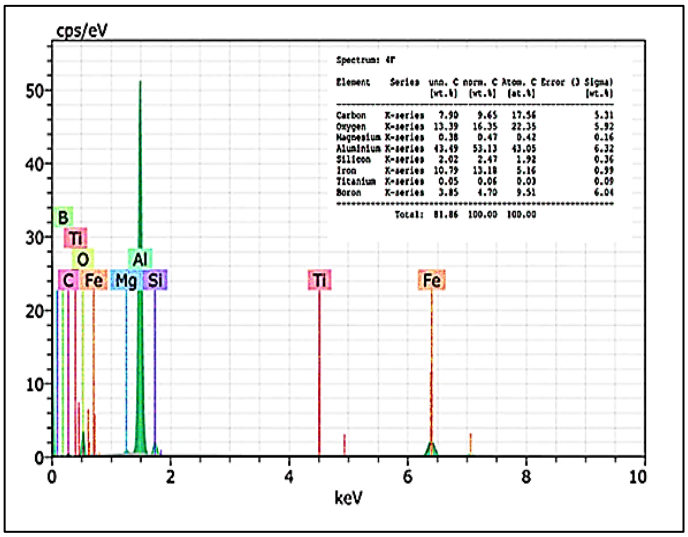

Fig. 22. EDS image spectra of (L= 20 N, S= 3 m/s and T= 60º C).

4.11. Determination of average wear rate and tensile strength response

The determination of average wear rate and tensile strength response at the optimal control settings within the specified (95% and 5%) confidence interval established by the equations for the confidence interval (CI), Eq.4 and Eq. (5) [57].

$$CI = \sqrt{F_{\alpha,1,Ve} \times V_{ep} \times \langle 1/n_{eff} | 1/R \rangle} \quad (4)$$

$$n_{eff} = \langle N | (1 + T_{dof}) \rangle \quad (5)$$

$F_{\alpha,1,Vep}$ =F ratio at the 95 % confidence level.
α =Significance level, Ve = Degree of freedom of the error.
V_{ep} =Error variance.
n_{eff} =Effective number of replications.
R = Number of replications for the confirmation test.

The predicted average wear rate and tensile strength response for the optimal control settings is $(R_o\text{-}CI)<Re<(R_o+CI) = -0.6541<2.76\times10^{-6}<0.6546$, where R_o is the optimum average wear rate and tensile strength response and R_e is the experimental value. Hence the average wear rate and tensile strength response at the optimal control settings within the specified confidence interval is validated.

4.12. Confirmation test

The confirmation tests were conducted with optimum parameters for wear rate arrived by MSEXCEL solver (Table 9). The error found to be less than 5%. The confirmation experiment for wear rate is also validated using confidence interval equations and F-test. Thus the dependability of the optimization is ensured. The graphical plot of wear (μm) against time (s) for the optimal control parameter settings is shown in Fig. 23. The amount of wear increases linearly with time. The amount of wear loss found to be less when compared to initial parameter settings of the experiment. The optimization results show considerable improvement in wear resistance under optimal conditions.

Table 9. Results of confirmation experiments.

Parameter	Optimal Conditions	Predicted value	Experimental value	Error
Wear Rate	A1,B3,C1 (10N,3m/s, 60º C)	0.000583	0.000612	4.73%

Fig. 23. Graphical plot of wear vs. time.

5. Conclusions

In the current research work, hybrid Al/B_4C/Fly ash composites were produced through the stir casting method and the effect of load, sliding velocity and temperature on the wear rate was evaluated. The following conclusions were drawn from the current research work.

- The microstructure analysis reveals the uniform distribution of reinforcement particles in the aluminium matrix. The hardness, compression and tensile strength of hybrid composites are higher compared to Al cast alloy and

Al/B_4C composites. The hardness of Al/B_4C/Fly ash is 28.19% higher when compared with cast aluminium alloy and 18.55% higher when compared with Al-B_4C composites. The ultimate tensile strength of hybrid composites increases by 21.9% when compared with Al cast alloy. The compression strength values of hybrid composites are 10% more compared to cast aluminium alloy.

- The grain structure was modified by the addition of strontium master alloy. With the addition of potassium flurotitanate (K_2TiF_6), bonding of boron carbide particles and fly ash particles with aluminium alloy matrix was improved. Magnesium powder is added to achieve good bonding and wettability.
- The wear rate increases with a rise in applied load and temperature and decreases with the increase in sliding velocity. Abrasive wear rises with a rise in temperature. The optimum wear rate occurs at 10 N load with sliding velocity 3 m/s and temperature 60ºC. From the ANOVA analysis, it was found that applied load (47.14%) is the highest significant parameter on the response, followed by temperature (40%) and sliding velocity (11.42%). Regression analysis revealed an extensive association between input parameters and response. The amount of wear loss found to be less under optimal conditions. Hence the Taguchi technique was used to predict the wear rate of Al-B_4C-FA composites effectively. The average wear rate and tensile strength response to the optimal control settings within the specified (95% and 5%) confidence interval is also validated by using F test. Similarly the reliability of the conformance test for wear rate is checked. The confirmation experiment results are also validated by the less error indicated.
- Al-B_4C-FA composites have promising application for use in the production of wear resistant automobile and aircraft parts capable of withstanding high temperature. The properties of Al-B_4C-FA composites further improved by choosing reduced fly ash particle size, coated boron carbide particles, intermetallics and Ti based master alloys.

References

1. Deborah, D.L. (2010). *Composite materials, science and applications*. Second Edition, Springer-Verlag London Limited.
2. Sastry, S.; Krishna, M.; and Uchil, J. (2001). A study on damping behaviour of aluminite particulate reinforced ZA-27 alloy metal matrix composites. *Journal of Alloys and Compounds*, 314(1-2), 268-274.
3. Michael, O.B.; Kenneth, K.; Alaneme, L.; and Heath, C. (2015). Aluminium matrix hybrid composites: a review of reinforcement philosophies; mechanisms, corrosion and tribological characteristics. *Journal of Material Research Technology*, 4(4), 443-445.
4. Terry, B.; and Jones, G. (1990). *In metal matrix composites-current developments and future trends in industrial research and applications*. Elsevier Advanced Technology Publication, Oxford, UK.
5. Kainer, K.U. (2006). *Metal matrix composite custom made material for automotive and aerospace engineering*. Wiley VCH Verlog GmbH & Co KGaA. Weinheim.

6. Rajan, T.P.D.; Pillai, R.M.; Pai, B.C.; Satyanarayana, K.G.; and Rohatgi, P.K. (2007). Fabrication and characterization of Al-7Si-0.35Mg/fly ash metal matrix composites processed by different stir casting routes. *Composites Science and Technology*, 67(15-16), 3369-3377.
7. Rohatgi, P.K.; Weiss, D.; and Gupta, N. (2006). Applications of fly ash in synthesizing low-cost MMCs for automotive and other applications. *JOM*, 58(11), 71-76.
8. Anilkumar, H.C.; Hebbar, H.S.; and Ravishankar, K.S. (2011). Mechanical Properties of fly ash reinforced aluminium alloy (Al6061) composites. *Journal of Mechanical and Materials Engineering (IJMME)*, 6(1), 41-45.
9. Swamy, A.R.K.; Ramesha, A.; Veeresh Kumar, G.B.; and Prakash, J.N. (2011). Effect of particulate reinforcements on the mechanical properties of Al6061-WC and Al6061-Gr MMCs. *Journal of Minerals and Materials Characterization and Engineering*, 10(12), 1141-1152.
10. Mummery, P.M.; Derby, B.; and Scruby, C.B. (1993). Acoustic emission from particulate reinforced metal matrix composites. *Acta Metallurgica*, 41(5), 1431-1445.
11. Zhu; H.X.; and Liu, S.K. (1993). Mechanical properties of squeeze cast zinc alloy matrix composites containing alpha-alumina fibers. *Composites*, 24(6), 437-442.
12. Rohtagi, P.K. (1994). Low-cost, fly-ash-containing aluminium matrix composites. *JOM*, 46(11), 55-69.
13. Rohtagi, P.K.; Guo, R.Q.; Huang, P.; and Ray, S. (1997). Friction and abrasion resistance of cast aluminium-fly ash composites: A review. *Metallurgical and Materials Transactions A*, 28(1), 245-250.
14. Dey, A.; and Pandey, Krishna, K.M. (2016). Characterisation of fly ash and its reinforcement effect on metal matrix composites. *Reviews on Advanced Material Science*, 44(2), 168-181
15. Venkat Prasat, S.; and Subramanian, R. (2013). Tribological properties of AlSi10Mg/Fly ash/graphite hybrid metal matrix composites. *Industrial Lubrication and Tribology*, 65(6), 399-408.
16. Sarkar, S.; Mohan, S.; and Panigrahi, S.C. (2008). Effect of particle distribution on the properties of aluminium matrix in-situ particulate composites. *Journal of Reinforced Plastics and Composites*, 27(11), 1177-1187.
17. Mahendra, K.V.; and Radhakrishna, K. (2007). Fabrication of Al-4.5% Cu alloy with fly ash MMC and characterization. *Materials Science-Poland*, 25(1), 57-68.
18. Kulkarni, S.G.; Menghani, J.V.; and Achchhe, L. (2016). Investigation of mechanical properties of fly ash and Al_2O_3 reinforced A356 alloy matrix hybrid composite manufactured by improved stir casting. *Indian Journal of Engineering and Materials Science*, 23(1), 27-36.
19. Shashi, P.D.; Satpal, S.; and Raghavendra, K.M. (2015). Microstructure and mechanical behaviour of A356/SiC/Fly ash hybrid composites produced by electromagnetic stir casting. *Journal of Brazilian Society of Mechanical Sciences and Engineering*, 37(1), 57-67

20. Lashgari, H.R.; Emamy, M.; Razaghian, A.; and Najimi, A.A. (2009). The effect of strontium on microstructure, porosity and tensile properties of A356-10% B_4C cast composites. *Material Science and Engineering*, 517(1), 170-179.
21. Srivastava, A.K.; Dixit, A.R.; and Tiwari, S. (2016). Investigation of micro-structural and mechanical properties of metal matrix composite A359/B_4C through electromagnetic stir casting. *Indian Journal of Engineering Material Science*, 23(2&3), 171-180.
22. Kalaiselvan, K.; Murugan, N.; and Parameswaran, S. (2011). Production and characterization of Al 6061-B_4C stir composite. *Materials and Design*, 32(7), 4004-4009.
23. Harun, M.B.; Shamsudin, S.R.; Yazid, H.; Selamat, Z.; Sattar, M.S. and Jalil, M. (2006). Microstructure porosity and hardness in Al-(Si-Mg) cast composites. *ASEAN Journal for Science and Technology Development*, 23(1&2), 113-122.
24. Toptan, F.; Kilcarselan, A.; Karaaslan, A.; Cigdem, M.; and Kerti, I. (2010). Processing and microstructural characterization of AA1070 and AA6063 matrix B_4Cp reinforced composites. *Materials & Design*, 31, Supplement 1, S87-S91.
25. Ramachandra, M.; and Radhakrishna, K. (2007). Effect of reinforcement of fly ash on sliding wear, slurry erosive wear and corrosive behaviour of aluminium matrix composite. *Wear*, 262(11-12), 1450-1462.
26. Charles, S.; and Arunachalam, V.P. (2004). Property analysis and mathematical modelling of machining properties of aluminium alloy hybrid (Al-alloy/SiC/fly ash) composites produced by liquid metallurgy and powder metallurgy techniques. *Indian Journal of Engineering & Material Sciences*, 11(6), 473-480.
27. Uthayakumar, M.; Thirumalai Kumaran, S.; and Aravindan, S. (2013). Dry sliding friction and wear studies of fly ash reinforced AA-6351 metal matrix composites. *Advances in Tribology*, Volume 2013 (2013), Article ID 365602, 6 pages.
28. Sudarshan; and Surappa, M.K. (2008). Synthesis of fly ash particle reinforced A356 Al Composites and their characterization. *Material Science and Engineering: A*, 480(1-2), 117-124.
29. Parathsarathi, N.L.; Borah, U.; and Alber, Sh.K. (2013). Correlation between coefficient of friction and surface roughness in dry sliding wear of AISI 316L(N) stainless steel at elevated temperatures. *Computer Modelling and New Technologies*, 17(1), 51-63.
30. Radhika, N.; Subramanian; and Venkat Prasat, S. (2011). Tribological behaviour of aluminium/alumina/graphite hybrid metal matrix composite using Taguchi's techniques. *Journal of Minerals and Materials Characterization and Engineering*, 10(5), 427-443.
31. Shanmughasundaram, P. (2017). Effect of temperature, load and sliding velocity on the wear behaviour of AA7075-SiC composites. *Mechanics and Mechanical Engineering*, 21(1), 85-93.
32. Natarajan, S.; Narayanasamy, R.; Kumaresh Babu, S.P.; Dinesh, G.; Anil Kumar, B.; and Sivaprasad, K. (2009). Sliding wear behaviour of

Al6063/TiB_2 in situ composites at elevated temperature. *Materials and Design*, 30(7), 2521-2531.

33. Das, S. (2004). Development of aluminium alloy composites for engineering applications. *Transactions of Indian Institute of Metals*, 57(4), 325-334.
34. Piyadeh, F.; Abdullah-Pour, H.; and Lieblich, M. (2014). Production of AA2124 /MoSi2/25p composites and effect of heat treatment on their microstructure, hardness and compression properties. *Revista De Metalurgia*, 50(4), e030, 1-8.
35. Roy, K.R. (1990). *A primer on the Taguchi method*. Van Nostrand Reinhold, New York, NY.
36. Mallapur, D.G.; Rajendra Udupa, K.; and Kori, A. (2010). Influence of Ti, B and Sr on the microstructure and mechanical properties of A356 alloy. *International Journal of Mechanical Engineering and Technology*, 1(1), 49-59.
37. Gikunoo, E.; Omotoso, O.; and Oguocha, I.N.A. (2005). Effect of fly ash particles on the mechanical properties of aluminium casting alloy A535. *Material Science and Technology*, 21(2), 143-152.
38. Shorowordi, K.M.; Laoui, T.; Haseeb, A.S.M.A.; Celis, J.P.; and Froyen, L. (2003). Microstructure and interface characteristics of B_4C, SiC and Al_2O_3 reinforced Al matrix composites: a comparative study. *Journal of Materials Processing Technology*, 142(3), 738-743.
39. Arslan, G.; and Kalemtas, A. (2009). Processing of silicon carbide-boron carbide-aluminium composites. *Journal of the European Ceramic Society*, 29(3), 473-480.
40. Auradi, V.; Rajesh, G.L.; and Kori, S.A. (2014). Processing of B_4C particulate reinforced 6061 Aluminium matrix composites by melt stirring involving two step addition. *3rd International Conference on Material Processing and Characterisation*, *Procedia Material Science*, Hyderabad, India, 1068-1076.
41. Suresh, N.; Venketeswaran, S.; and Seetharamu, S. (2010). Influence of cenpspheres of fly ash on the mechanical properties and wear of permanent moulded eutectic Al-Si alloys. *Materials Science-Poland*, 28(1), 55-65.
42. Alizadeh, M.; and Paydar, M.H. (2010). Fabrication of nanostructure Al/SiCp composite by accumulative roll bonding (ARB) process. *Journal of Alloys and Compounds*, 492(1-2), 231-235.
43. Shin, J.H.; Choi, H.J.; and Bae, D.H. (2014). The structure and properties of 2024 aluminium composites reinforced with TiO_2 nanoparticles. *Materials Science and Engineering: A*, 607, 605-610.
44. Alaa, M.R.; Dayang, L.M.; Mohamad, R.I.; and Uday, M.B. (2017). Effect of fly ash addition on the physical and mechanical properties of AA6063 Alloy reinforcement. *Metals*, 7(11), 477, 1-15.
45. Mazaheri, Y.; Karimzadeh, F.; and Enayati, M.H. (2014). Tribological behaviour of A356/Al_2O_3 surface nanocomposite prepared by friction stir processing. *Metallurgical and Materials Transactions* A, 45(4), 2250-2259.
46. Ravi Kumar, K.; Mohanasundaram, K.M.; Aramaikkannu, G.; and Subramanian, R. (2012). Effect of particle size on mechanical properties and tribological behaviour of aluminium/fly ash composites. *Science and Engineering Composite Materials*, 19(3), 247-253.

47. Li, R.-X.; Li, R.-D.; and Bai, Y.-H. (2010). Effect of specific pressure on microstructure and mechanical properties of squeeze casting ZA27 alloy. *Transaction of Nonferrous Metals Society of China*, 20(1), 59-63.
48. Baradeswaran, A.; Elaya Perumal, A.; and Davim, J.P. (2013). Effect of B_4C on Mechanical properties and Tribological behaviour of AA 6061-B_4C Composites. *Journal of the Balkan Tribological Association*, 19(2), 230-239.
49. Al-Araji, N.; and Sarhan, H.S. (2011). Effect of temperature on sliding wear mechanism under lubricated conditions. *International Journal of Engineering*, 5(2), 176-184.
50. AI-Qutub, A.M.; Allam, I.M.; and Abdulsamad, M.A. (2008). Wear and friction of Al-Al_2O_3 composites at various sliding speeds. *Journal of Materials Science*, 43(17), 5797-5803.
51. Lindros, M.; Apostol, M.; Heino, V.; Valtonen, K.; Laukkanen, A.; Holmberg, K.; and Kuokkala, V.T. (2015). The deformation, strain hardening, and wear behaviour of chromium-alloyed hadfield steel in abrasive and impact conditions. *Tribology Letters*, 57(3), 1-17.
52. Radhika, N.; Vaishnavi, A.; and Chandran, G.K. (2014). Optimisation of dry sliding wear process parameters for aluminium hybrid matrix composites. *Tribology in Industry*, 36(2), 188-194.
53. Zhu, H.; Sun, X.; Huang, J.; Li, J.; and Xie, Z. (2017). Dry sliding tribological behaviour at elevated temperature of in situ aluminium matrix composites fabricated by Al-ZrO_2-C system with different mole ratio of C/ZrO_2. *Journal of Powder Metallurgy and Mining*, 6(1), 1-5.
54. Rohatgi, P.K.; and Guo, R.Q. (1997). Low cost cast aluminium-fly ash composites for ultralight automotive application. *TMS Annual Meeting, Automotive Alloys*, 157-168.
55. Radhika, N.; Balaji, T.; and Palaniappan, S. (2015). Studies on mechanical properties and tribological behaviour of LM25/SiC/Al_2O_3. *Journal of Engineering Science and Technology* (*JESTEC*), 10(2), 134-144.
56. Dixit, G.; and Khan, M.M. (2014). Sliding wear response of an aluminium metal matrix composite: Effect of solid lubricant particle size. *Jordan Journal of Mechanical and Industrial Engineering*, 8(6), 351-358.
57. Mandal, N.; Doloi, B.; Mondal, B.; and Das, R. (2011). Optimization of flank wear using Zirconia Toughened Alumina (ZTA) cutting tool: Taguchi method and regression analysis. *Measurement*, 44(10), 2149-2155.